Strength and crashworthiness of aircraft composite FRP panels under blast and explosion

João Néné
joaonene@tecnico.ulisboa.pt

Instituto Superior Técnico, Universidade de Lisboa, Portugal

April 2021

Abstract

Carbon fibre-reinforced polymer (CFRP) composite laminates are increasingly being used in aerospace structures (e.g., fuselage panels) at risk of blast actions. This study aims to numerically investigate the influence of the curvature and stiffeners' geometry on the mitigation of the effects of a shock wave loading in single-curved CFRP panels. Initially, a numerical model of a flat CFRP panel was developed and validated. Then, the dynamic response and blast resistance of curved panels (without and with reinforcements) was studied, capturing the deformation patterns and failure modes, as well as the influence of strain rate on the material properties. The results showed that the blast resistance of the panels is sensitive to the geometry of the incident surface: the convex configuration shows higher resistance to blast loading than its concave counterpart. For blast conditions below a loading threshold, the increase of the curvature resulted in a higher dissipation of the loading from the shock wave due to the higher angle of incidence. Additionally, the deformations also decreased due to an increase of the geometric stiffness of the panels. Finally, the addition of structural reinforcements was proven to reduce both maximum deformation of the panels and damage of the laminates, with the Ω-shaped stringers outperforming the remaining ones studied.

Keywords: Blast loading, CFRP curved stiffened panels, numerical model, dynamic response, failure mechanisms

1. Introduction

Civil aviation has been a target for acts of aggression and terrorism since the beginning of the 20th century. A series of attacks throughout the years has shown the vulnerability of civilian aircraft to the blasts caused by in-cabin explosions. Aerospace structures, and more specifically aircraft fuselages, are subjected to a complex combination of loads and their design must follow conflicting requirements of strength, stiffness and weight. In this context, composite materials have become popular over the years, increasingly being used in a wide range of structural applications due to their advantages over conventional metal alloys [1]. The main drawback that the use of composite materials present is their brittle response specially under high strain-rate loading events. In the case of a shock wave generated by an explosion, composites exhibit poor matrix dominated properties in the transverse direction and weak through thickness properties. Moreover, while conventional metals (i.e., steel and aluminium alloys) have the ability to absorb a large amount of energy as they plastically deform, fibre-reinforced polymer (FRP) laminates experience a series of complex brittle-like damage processes under explosive blast loading such as matrix cracking, delamination and fibre fracture at much lower strains.

A large body of work into the blast response of panels has been published, focusing mainly on the response of metal-based composite materials [2–5]. While there are finite element models capable of assessing the deformation blast loading in these surfaces, the lack of literature regarding the field of composite materials, especially concerning the strain-rate sensitivity of FRP composites at high strain-rates induced by blast loading, presents a challenge to numerical modelling. In recent years, experimental and numerical investigations into the deformation and failure process of FRP composites in air blasts have been published, almost entirely restricted to flat configurations [6–8], with few studies addressing the dynamic response of fibre-reinforced curved panels [9]. Recently, however, the interest in curved panels for blast mitigation purposes has increased due to the additional stiffness under explosive blast loads by virtue of their spatial

curvatures [2]. At the time of writing this work, no research into the blast response of structurally-reinforced CFRP curved panels is available in the literature.

This work aims to contribute to a better understanding of the effects of the complex nature of blast actions on carbon fibre-reinforced polymer (CFRP) laminate single-curved panels representative of a fuselage section, through a numerical investigation. Abaqus/Explicit (version 6.14) is used to assess the deformation patterns and failure modes of the panels and the influence of geometric parameters (i.e., curvature and reinforcement's shape) on the mitigation of the effects of a shock wave loading during a bombing event. In this work, an overview of the underlying theory regarding the response of FRP panels to explosive blast loading is presented (Section 2). A detailed description of the numerical models developed is covered (Section 3). Lastly, the results are reported and discussed (Section 4) and the conclusions are presented (Section 5).

2. Background

2.1. Explosive blast loading

The blast caused by the detonation of conventional explosives originates a localized release of energy in which the highly compressed and hot gases expand, resulting in a shock wave. The shock wave expands rapidly, propagating at a speed faster than the speed of sound, causing an almost instantaneous change in overpressure, followed by an exponential decay modeled by the Friedlander's equation [10],

$$P_s(t) = P_{so}\left(1 - \frac{t}{t_d}\right)e^{-b\frac{t}{t_d}}, \qquad (1)$$

where P_s is the overpressure at a time instant t, P_{so} is the peak overpressure, t_d is the duration time (until the overpressure reaches ambient pressure, after the wave front) and b is the decay coefficient.

The time period between the time of arrival of the shock wave (t_A) and t_d, makes the positive pressure phase. After this point, the overpressure decreases further until it stabilizes. The later phase, know as negative pressure phase, is longer in duration, but much lower in amplitude than the positive phase and can often be neglected [11].

The main parameters that define a blast loading are the relative distance between the detonation point and the structure of interest, know as stand-off distance (SOD), the mass and type of explosive and the geometry of the target structure. For conditions under which the target structure is located within the fireball resulting from the detonation of an explosive charge, the expanding gas products dominate the loading and the shock wave can be neglected. Under this condition, the explosion is deemed as near-field. When the target is outside the fireball (typically at a distance within 10 to 20 times the radius of a spherical charge), the effects of the fireball can be disregarded and the explosive event is considered far-field [6]. Different types of blasts can be considered, depending on the relative position of the explosive source and structure and the distance above ground. In free-air blasts, considered in this work, the shock wave propagates spherically outwards and interacts directly with the structure, with no influence of second-order reflections due to the surroundings.

Several approaches can be used when modelling the detonation of an explosive charge. Kingery and Bulmash [12] developed charts based on experimental studies to obtain the blast parameters from explosive tests using charges of TNT for both free-air and surface blasts. Using this data, high-order polynomial equations can be fitted to describe the overpressure-time profile of a blast wave. CONWEP (Conventional Weapons Effects Programme) is the most recognised empirical model implemented in finite elements commercial codes such as Abaqus/Explicit and allows to realistically simulate overpressure amplitudes (including positive and negative phases) and does not require a fluid medium to account for shock wave propagation, resulting in an accurate and computationally efficient approach to model an explosive blast [11]. However, it is unable to account for the phenomena associated to near-field and semi-confined blasts, which include the effects of reflective waves and fireballs during an explosion.

2.2. FRP composite laminates

Classical Laminate Theory is used in the analysis of fibre-reinforced composites and defines the response of a laminate. Constitutive equations allow to predict strains and stresses by defining the engineering constants associated to an orthogonal local coordinate system with the 1-axis in the fibre direction, the 2-axis perpendicular to the fibres on the plane of the lamina and the 3-axis perpendicular to the plane of the lamina. For composite laminate panels, the thickness of each single unidirectional ply is small when compared to the panel dimensions and a plane stress condition can be applied [1].

Hashin failure criteria, which is based on the work of Hashin and Rotem [13] and Hashin [14], is implemented in Abaqus [15] to model four intralaminar damage initiation mechanisms that include fibre rupture in tension (F_f^t), fibre kinking in compression (F_f^c), matrix cracking in tension (F_m^t) and matrix crushing in compression (F_m^c), defined for plane stress conditions as follows,

$$F_f^t = \left(\frac{\hat{\sigma}_{11}}{X_T}\right)^2 + \alpha\left(\frac{\hat{\sigma}_{12}}{S_L}\right)^2 \quad \text{if} \quad \hat{\sigma}_{11} \geq 0, \tag{2}$$

$$F_f^c = \left(\frac{\hat{\sigma}_{11}}{X_C}\right)^2 \quad \text{if} \quad \hat{\sigma}_{11} < 0, \tag{3}$$

$$F_m^t = \left(\frac{\hat{\sigma}_{22}}{Y_T}\right)^2 + \left(\frac{\hat{\sigma}_{12}}{S_L}\right)^2 \quad \text{if} \quad \hat{\sigma}_{22} \geq 0, \tag{4}$$

$$F_m^c = \left(\frac{\hat{\sigma}_{22}}{2S_T}\right)^2 + \left[\left(\frac{Y_C}{2S_T}\right)^2 - 1\right]\frac{\hat{\sigma}_{22}}{Y_C} + \left(\frac{\hat{\sigma}_{12}}{S_L}\right)^2 \quad \text{if} \quad \hat{\sigma}_{22} < 0. \tag{5}$$

In equations (2) to (5), X_T, Y_T, X_C and Y_C denote the allowable tensile (T) and compressive (C) strengths in the material directions (X - direction of fibres and Y - direction perpendicular to the fibres), S_L and S_T are the allowable longitudinal and transverse shear strengths, respectively, and the coefficient α determines the contribution of the shear stress to the fibre tension damage criteria. The initiation criteria presented can be used to obtain the model proposed in Hashin and Rotem [13] by setting $\alpha = 0.0$ and $S_T = Y^C/2$ or the model proposed by Hashin [14] by setting $\alpha = 1.0$. When any of the failure indices (F_f^t, F_f^c, F_m^t and F_m^c) reaches unity, the damage initiation criterion is met and the evolution of damage follows a damage evolution law, defined by specifying the fracture energies for fibre tension, fibre compression, matrix tension and matrix compression failure modes (G_{ft}^{cr}, G_{fc}^{cr}, G_{mt}^{cr}, and G_{mc}^{cr}, respectively).

The behaviour of cohesive zones used to model bonded interfaces is defined by an elastic constitutive matrix that relates the normal and shear stresses to the normal and shear displacements in terms of traction-separation laws that assume a linearly elastic behaviour followed by the initiation and evolution of damage. A maximum nominal stress criterion (MAXS) is used in the scope of this work to define the initiation of cohesive damage, which is given by

$$\max\left\{\frac{t_n}{t_n^o}, \frac{t_s}{t_s^o}, \frac{t_t}{t_t^o}\right\} = 1, \tag{6}$$

where t_n, t_s and t_t are the three components of the nominal traction stress vector and the subscripts n, s and t denote the normal and two shear tractions, respectively. The stress values t_n^o, t_s^o and t_t^o represent the maximum values of the nominal stress when the deformation is applied normal to the interface or in the first and second shear directions, respectively.

Damage growth is defined by the rate of stiffness degradation which is expressed in the form of a damage evolution law. In this work, the damage evolution law given by the Benzeggagh-Kenane (BK) criterion is considered, which is based on the dependence of the fracture energy on the damage made and takes the the following form,

$$G_n^{cr} + (G_s^{cr} - G_n^{cr})\left\{\frac{G_S}{G_T}\right\}^{\eta} = G^C, \tag{7}$$

where $G_S = G_s + G_t$ and $G_T = G_n + G_S$.

G_n^{cr}, G_s^{cr} and G_t^{cr} are the critical fracture energies values in modes I, II and III, respectively, which are predicted by the fracture mechanics theory with respect to the three modes of failure to propagate in a material due to tensile and shear stresses. G_n, G_s and G_t refer to the work done by the traction and its conjugate relative displacement in the normal, first and second shear directions, respectively. η is a material parameter and G^C is the mixed-mode fracture energy.

3. Numerical model

3.1. Geometry and finite element mesh

The panels studied in this research consist of variations of a reference panel which incorporates five evenly-spaced T-shaped longitudinal stringers bonded to a cylindrical skin by an adhesive layer, shown in Figure 1 [16–18].

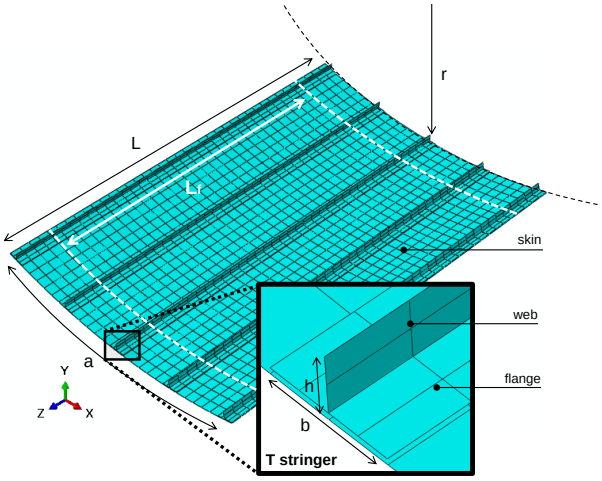

Figure 1: Geometry and mesh of the reference panel.

The panel has a total length L = 780 mm and a free length L_f = 660 mm. The arc length is a = 560 mm and the radius of the panel is r = 1000 mm. The flange of the T-shaped stringers has a width of b = 32 mm and the web a height of h = 14 mm. The skin and stringers are made of the same unidirectional (UD) fibre-reinforced laminae with thickness t = 0.125 mm, giving the skin, the stringers' flange and web a total thickness of 1, 1.5 and 3 mm, respectively. The stacking sequences of the skin, stringer flanges and stringer webs are $[90,+45,-45,0]_s$, $[(+45,-45)_3,0_6]$ (from top

to bottom) and $[(+45,-45)_3,0_6]_s$, respectively. In the stacking labeling, the subscript s means that the stacking sequence is symmetric with respect to the mid-plane of the referred laminate and the numerical subscript gives an indication on the number of times a given orientation or sequence of orientations is repeated.

In order to study the influence of the curvature on the blast response of the CFRP panel, three models were considered, which consisted of an unreinforced skin with varying radius of curvature (500, 750 and 1000 mm). The remaining parameters followed the geometric data of the reference panel. To take into account the influence of reinforcements, stringers with four other cross-section geometries (I-, C-, J- and Ω-shaped) were added into the model. The geometry and mesh data of the stringers' cross-section is depicted in Figure 2.

The skin and stringers of the panels were discretized with 4-node shell elements (named S4 in Abaqus nomenclature [15]). Each node of the S4 elements has six degrees of freedom (DOF), consisting of a displacement and a rotation for each one of the three directions of the global coordinate system. The mesh density was chosen upon a convergence analysis and four different meshes for the skin have been considered (ranging from 70 up to 4368 elements). The skin was subjected to the blast loading from an explosive charge of 100g of TNT, located at 1m normally from the panel's centre point. The degree of accuracy of the mesh was analysed in terms of the normal displacement in the centre point of the panel for a given (always the same) time instant. The converged element size was estimated to be 20mm, which resulted in 1092 elements and 1160 nodes in the skin of the panel as shown in Figure 1.

The mesh of the stringers was chosen based on the contact modeling approach used on the interface between the skin and stringers. Contact pairs defined under the general contact option in Abaqus/Explicit use a master/slave contact algorithm in which the nodes on the slave surface cannot penetrate the segments that make the master surface. For that reason, the slave surface should be the more refined surface [15]. In the models, the surface of the stringers was selected as the slave surface and therefore presents a finer mesh. For the reference panel, the mesh of the T-shaped stringers was set to have 2 elements along the height of the web and 4 elements along the width of flange, making a total of 234 elements and 280 nodes for each stringer (Figure 1). The remaining configurations followed the same criteria, with the mesh densities for each design being shown in Figure 2. The mesh of the surfaces of the flanges and webs comprise a total of 40 nodes along the longitudinal direction, the same as the mesh of the skin.

3.2. Materials

The unidirectional (UD) CFRP IM7/8552 (Carbon/Epoxy) adopted in the modelling of the panel's skin and stringers and the adhesive Redux 312 used in the bonded surfaces were chosen in virtue of their usage in the COCOMAT project [16] and following works [17–19]. The material parameters necessary to define the lamina-type material model in Abaqus are shown in Table 1. Intralaminar damage to the fibers and matrix was modelled using the Hashin failure initiation criterion for fibre-reinforced materials and the evolution of damage was implemented through a damage evolution law, described in Section 2. In this work, α was set to 1 in order to take into account the effect of shear on the fibre damage initiation. The parameters of the damage model shown in Table 1 include the Young's modulus (E_i), Poisson's ratio (ν_{ij}), shear modulus (G_{ij}), the tensile and compressive strengths (denoted by the subscript T and C, respectively) in the fibre and matrix directions (X and Y, respectively) and the fracture energies for each one of the failure modes, i.e., fibre tensile, fibre compressive, matrix tensile and matrix compressive (G^{cr}_{ft}, G^{cr}_{fc}, G^{cr}_{mt} and G^{cr}_{mc}, respectively).

The material properties are specified according to the material directions (i, j = 1, 2 or 3), which are defined by the reference orientation in the layup (1 $\equiv$ Z, 2 $\equiv$ X and 3 $\equiv$ Y for the skin and stringer's flanges and 1 $\equiv$ Z, 2 $\equiv$ Y and 3 $\equiv$ X for the stringer's webs (with the global coordinate system (X, Y and Z) represented in Figure 1)) and the relative rotation of the fibres.

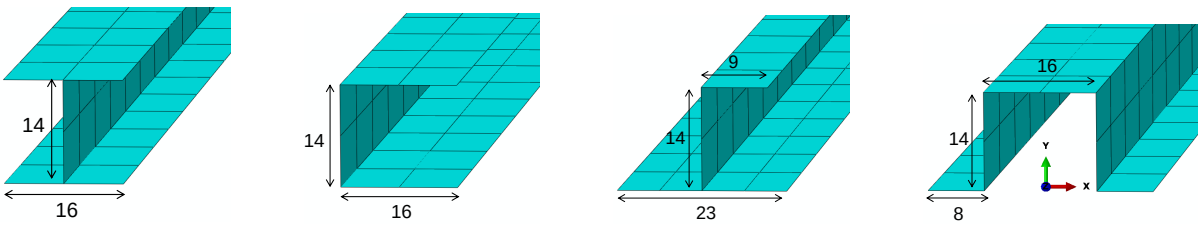

(a) I-shaped (b) C-shaped (c) J-shaped (d) Ω-shaped

Figure 2: Geometry and mesh of the I-, C-, J- and Ω-shaped stringers (dimensions in mm).

Table 1: Material parameters for the CFRP IM7/8552 UD lamina [16, 20, 21].

Elastic properties		Strength parameters	
E_1 [MPa]	147000	X_T [MPa]	2715
E_2 [MPa]	11800	X_C [MPa]	1400
ν_{12} [-]	0.34	Y_T [MPa]	56
G_{12} [MPa]	6000	Y_C [MPa]	25
G_{13} [MPa]	6000	S_L [MPa]	101
G_{23} [MPa]	4000	S_T [MPa]	131
Fracture energies			
G_{ft}^{cr} [N/m]	81500		
G_{fc}^{cr} [N/m]	106300		
G_{mt}^{cr} [N/m]	277		
G_{mc}^{cr} [N/m]	788		

The adhesive Redux 321 was modelled using a cohesive contact behaviour which follows the formulae and laws that govern cohesive constitutive behavior, including the linear elastic traction-separation model, damage initiation criteria and damage evolution laws described in Section 2. The cohesive interface is defined as part of the surface interaction property in Abaqus. The elastic properties were defined by the stiffness coefficients of the adhesive layer (K_{nn} = 15000 MPa/mm, K_{ss} = 5355 MPa/mm and K_{tt} = 5355 MPa/mm), obtained by dividing the material stiffness [16, 17] by the thickness of the adhesive t_a = 0.2 mm [15]. The maximum nominal stress criterion was used to predict the initiation of cohesive damage in the adhesive, which is defined by the maximum values of the normal and shear stresses in the cohesive interface (t_n^0, t_s^0 and t_t^0). The Benzeggagh-Kenane (BK) criterion was used as a damage evolution law with a power coefficient of 4.5 [22] and the normal and shear modes fracture energies of 200 and 1000 N/m [16], respectively.

3.3. Strain rate

An important consideration in blast modelling is the strain rate ($\dot{\varepsilon}$) sensitivity of the composite material. Studies have found changes in the material properties of composite laminates by up to 50% under the range of strains induced by blast loading, typically in the range of 100-1000 s^{-1} [7]. The exclusion of rate dependency is a shortcome of the default lamina-type material model of Abaqus used in the present work. As such, the following approach was used to qualitatively capture the influence of strain rate in the models [19].

First, the material property values at a quasi-static strain rate were used to model the panels. When subjected to a blast loading, the in-plane components of the strain-rate ER_{ij} tensor were used to obtained a unified value. Then, an average value of strain-rate was calculated, considering a time domain from the time of arrival of the shock wave up to the initiation of damage of the first failure mode according to Hashin's criteria (the null values were disregarded). The matrix-dominated properties of the IM7/8552 at the average strain-rate were given by the relations of the strain-rate-dependent behaviour of the material given in the work of Schaefer et al. [23]. Finally, a new model was created with the strain-dependent values of the material properties and subjected to the same blast conditions.

3.4. Blast loading and boundary conditions

The CONWEP model implemented in the Abaqus/Explicit software was adopted to simulate the blast loading in virtue of its accuracy and computational efficiency, especially for free-air (i.e., when there is no interference from reflective surfaces or shadowing objects) and far-field (i.e., when the effects of the dynamic pressure and explosive fireball can be disregarded) blast conditions [11]. The pressure-time profile of the shock wave is obtained based on the user-defined parameters (equivalent mass of TNT, spatial coordinates of the reference point and type of blast (set as free-air detonation in the current work)) and angle of incidence, and applied as a pressure load directly onto the surface.

The boundary conditions were set to approximate the constraints used in the previous studies involving these panels [17–20] and do not reflect the structural response of the panel when incorporated on the fuselage of an aircraft. Hence, the curved edges of the panels were clamped (with all 6 DOF restrained). Two sets of nodes comprising the first 60 mm (along the Z axis) from each end and across all the width (X axis) were only allowed to displace axially and transversely (in the Z and X-direction, respectively), with the remaining displacement and all rotations restricted. The edges within the free length, L_f, were set free.

3.5. Validation of the numerical model

The experimental and numerical investigations into the blast response of FRP laminates performed by Gargano et al. [7, 8] were used to validate the numerical model, as it follows similar modelling options as those used in this work in terms of blast conditions and material properties.

The CONWEP model was capable of obtaining, with good accuracy, the overpressure-time profiles of the shock wave for far-field conditions, with the peak overpressure presenting differences between 1.43% and 4.80% (Figure 3). However, it becomes less accurate with reduced stand-off distances, particularly for near-field conditions.

The maximum center-point displacement history shows a good agreement for the initial deflection of the plate. After a certain instant, the agreement is poor, being increasingly less accurate for

higher impulse levels, mainly due to the omission of material damping and simplifications in the boundary conditions of the model. For low blast impulses (i.e., in far field conditions), the FEM accurately predicts the impulses (with a maximum difference of 10%) for the same test conditions. The displacement follows a linear variation, with the maximum centre-point displacement presenting a variation within 11%. In near-field conditions, however, CONWEP over-predicts the impulses generated by the shock wave which leads to higher maximum out-of-plane displacements, as seen in Figure 4.

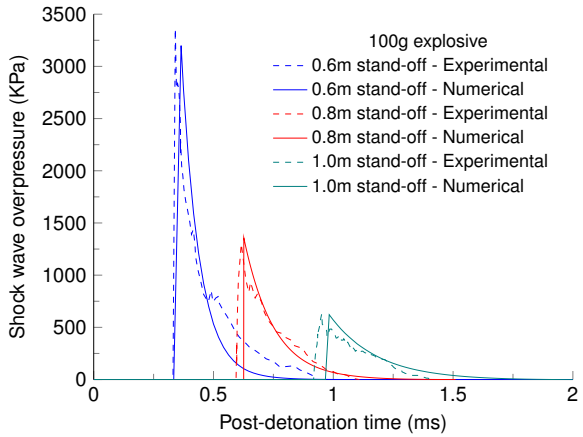

Figure 3: Far-field measured (dashed lines) and numerical (solid lines) overpressure-time profiles.

Damage initiation was modelled using Hashin's damage initiation criteria. The model predicted with accuracy the initiation and progression sequence of the damage modes identified by Gargano et al. [7], namely matrix crushing and cracking and fibre kinking and rupture, at several discrete regions in the plate edges, which rapidly propagated towards the centre.

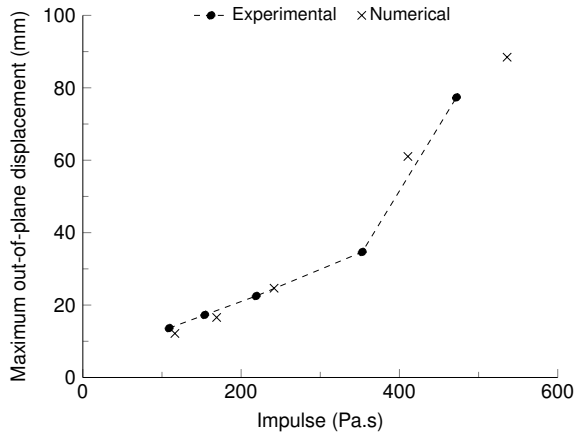

Figure 4: Effect of blast impulse on the maximum out-of-plane displacement.

In the experimental and numerical investigations [7,8], rupture in the plies was observed for the highest blast impulses. In the models developed in this work, the regions where rupture in the plies was observed matched with the elements in which the damage variables for all four failure modes reached unity (i.e., the elements offered no resistance to further deformation). As the FEM cannot predict delamination, no further discussion of delamination as a failure mode is thus carried in this work.

The proposed numerical model successfully incorporates most of the key aspects of the deformation and failure mechanisms during the blast loading of a CFRP laminate under certain blast conditions, hence supporting the use of the methodology proposed in the study of composite structures subjected to explosive blast events.

4. Results and discussion

4.1. Dynamic response analysis

In this section, the dynamic response of the curved CFRP panel with the reference geometry and without reinforcements is presented. The blast conditions (mass of TNT of 100 g and stand-off distance, SOD, of 1 m, normal to the centre-point of the panel) were chosen in virtue of the accuracy of the CONWEP model in simulating the overpressure-time profiles of blast waves in far-field conditions. The shock wave loading was applied on both the concave and convex surfaces.

For both (concave and convex) cases, the spherical propagation of the shock wave front and geometry of the incident surface result in distinct distributions of loads and, consequently, deformation patterns on the panel. In the convex specimen, two regions of response were identified. First, the localised nature of the blast load results in a bounded deformation pattern in the form of indentation, leading to an increase of the deformation in the centre region of the panel, which gives rise to high strains in the very first part of the blast event (when the pressure loading is the highest). The deformation progressively increases from the centre to the edges, along the circumferential (X) and longitudinal (Z) axis, and the indentation mode is replaced by a global response which comprises two deformation regimes in the form of bending and stretching. For the concave case, the shock front firstly acts on a "strip" along the curvature of the panel, propagating along the longitudinal axis. In this case, the indentation regime previously mention is not observed. This results in the highest values of out-of-plane displacements to be found in the free edges of the panel and a more unidirectional distribution of the stresses along the surface.

As the structures deform, there is a rapid degradation of the strength and reduction of the resistance to deformation of the panels due to the initiation of damage. The regions of response within the panel surface during the blast event result in

different damage patterns depending on the geometric configuration and ply orientation. For both cases, the extent of damage associated with matrix failure is higher than that observed for fibre failure, as the strength parameters associated with matrix failure are lower when compared to the fibre strengths. The distribution of damage in the surfaces followed the deformation patterns previously observed and is influenced by the degradation of element strength due to the contributions of bending and membrane stresses in the local and global regions of the response of the panel. The panels were found to go from a bending dominated to a coupled bending-stretching regime, as the reaction forces in the fixed boundaries alternated from a compressive to a tensile force during the blast event. Matrix damage initiated in the fixed boundaries of the panel for both configurations and progressed along the areas with higher deformation. The diffusion of the effects from the shock wave loading accomplished by the convex surface, however, effectively delayed the initiation of fibre damage and reduced the extent of fibre-damaged elements, which are found in the centre region at the end of the blast loading, at an instant in which the panel is at its maximum deflection. The concave surface favours the initiation and propagation of fibre damage along the fixed edges of the panel, leading to a rapid degradation of the structural integrity and consequently collapse of the panel, shortly after the shock wave loading.

An energy analysis allowed to assess the dynamic response and accuracy of the numerical model. The elastic strain energy (E_{SE}) gives an indication of the deformation of the panels during the elastic regime (Figure 5). The deformation is built up until a point of maximum deflection is reached, in which the value of E_{SE} is maximum and the panel is almost entirely at rest, causing the kinetic energy (E_{KE}) to be at a minimum. Although this relation is observed in the convex case, the concave specimen shows a local maximum value of E_{SE} earlier in the blast event (prior to the first local minimum of E_{KE}). The concave model shows higher values of energy dissipated by damage (E_{DMD}), mainly attributed to the higher extent of fibre-damaged elements, when compared to the convex case. As the blast-induced damage increases, the loss of strength in the damaged elements reduces the ability of the panels to withstand further deformations, reducing the capability of decreasing E_{KE} and ultimately leading to collapse. As the CFRP panels are mainly able to dissipate energy via damage and damping due to viscous effects, the elastic brittle behaviour observed shows a conflict when using composites at risk of explosive blast, as the inability to dissipate energy due to plastic deformation restricts the capability to limit the penetration and damage whilst maximizing energy absorption. The energy conservation of the model was investigated and the total energy was found to be approximately constant, as it should [15]. Moreover, the ratio of artificial strain energy (E_{AE}) to the internal energy was found to be below the threshold of 5% used to evaluate the accuracy of numerical models [15].

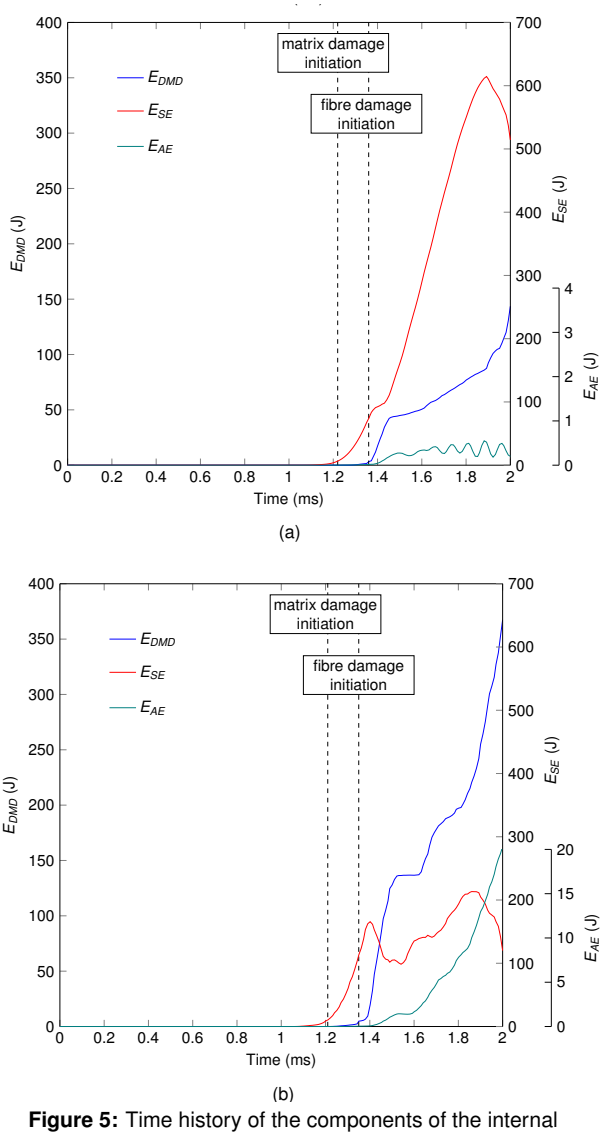

Figure 5: Time history of the components of the internal energy for the (a) convex and (b) concave configuration.

4.2. Influence of panel curvature on the blast response

For the purpose of analysing the effect of the curvature on the resistance of CFRP panels to blast loading, a group of panels with different radii of curvature (500, 750 and 1000 mm) but with the same mass and section area was investigated. The panels were subjected to the shock waves resulting from the explosive blast of two distinct charges,

60 g and 100 g of TNT, located at the same detonation point as previously.

The work of the external loads, E_{WK}, for each panel gives an insight on the influence of curvature on the blast response of the panels, as seen in Figure 6. The curvature of the panels changes the reflective angle of the shock wave, used by CONWEP to calculate the pressure loading. Bigger radii of curvature (i.e., flatter surfaces) result in a smaller reflective angle and, therefore, higher values of pressure loading applied on the surfaces. Moreover, by increasing the curvature of the panels, the stiffness (which is function of the area moment of inertia) also increases, resulting in lower average displacements with increasing curvatures. Another observation is that the blast mitigation properties in virtue of the increased curvature on the panels will be more significant with increasing blast loads, as the trend lines for each mass of explosive charge show that the slope of the linear regression for 100 g of TNT is higher (by about 43%) than for 60 g.

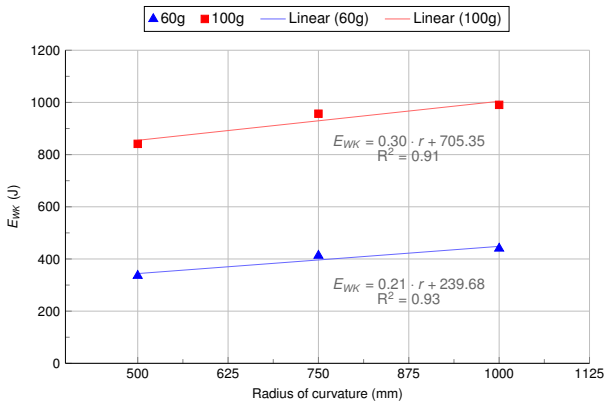

Figure 6: Maximum value of E_{WK} vs. radius of curvature, r, for charge masses of 60g and 100g of TNT.

The previous observations translate into the panel with highest radius of curvature (R1000) showing the highest values of E_{KE} and the R500 panel showing the lowest (for both blast conditions). Moreover, the fact that, under both blast conditions, the panels show a first local maximum value of E_{SE} at a very early stage in the blast event is indicative of a significant contribution of the damage in the dynamic response of the panels, irrespective of the radius of curvature.

The initiation of damage depends on the dynamic response of the panels, as stresses will concentrate in the areas where higher deformations are found. The curvature is seen to originate different deformation patterns, with higher displacements found on the free edges with increasing curvatures and similar deformed shapes on the longitudinal direction. Moreover, the geometric stiffness induced by the curvature favours higher stresses on the surface of the panels as further bending is limited by the increased stiffness of the structures.

All four failure modes were identified and it was observed that the curvature influences the initiation of a particular failure mode whilst maintaining the same sequence (damage due to matrix tension, matrix compression, fibre tension and fibre compression). In all panels it is observed that the damage progressed from the boundary of the laminates to the centre, with the damage associated with the two matrix failure modes being dominant. As the curvature increases, a predisposition towards more damage on the free edges becomes more evident. By decreasing the curvature, however, the damage spreads towards the centre of the panel, complementing the higher displacements found in this area. The extent of the damaged areas in the panels under the same blast loading condition is very similar, irrespective of radius of curvature. For a charge mass of 100 g, the panels were found to collapse at sensibly the same time. The decrease in the extent of damage with regards to both the matrix and fibre damage modes for the lowest mass charge (60 g) resulted in the preservation of the structural integrity of the panels.

Thus, it is possible to ensure that, for certain blast conditions below a loading threshold, the panel with higher curvature outperforms the remaining geometries, as it shows a higher capability to mitigate the loading under an explosive blast event, while showing an increased geometric stiffness that reduces the deformations. For higher values of load, however, in conditions under which the panels collapse, the increase in curvature does not offer an additional benefit for blast mitigation purposes.

4.3. Influence of structural reinforcements

In order to study the influence of stringer cross-section geometry on the blast performance of the reference panel, four additional cross-sectional shapes were considered (T-, I-, C-, J- and Ω-shaped) and subjected to the same far-field conditions as previously (W_e = 100 g, SOD = 1 m).

The introduction of longitudinal stringers in the panels resulted in an increased flexural stiffness which resulted in lower values of deformation throughout the blast event. Despite the deformation pattern of the panels being qualitatively identical, stringer geometry alters the projected area of the panel which will be under the influence of the blast loading and the deformation modes observed. As such, at the same post-detonation time instant prior to damage initiation, the panel with Ω-shaped stringers displays the lowest values of out-of-plane displacement in the skin, and the panel

with C-shaped stringers the highest. In the latter case, a coupled bending-torsion mode is observed in virtue of the cross-section's asymmetry (in which the shear centre and centroid of the stringers are not aligned).

The addition of stringers into the panels results in a significant reduction of E_{KE}. The stringers increase the mass of the panels in about 1.8 times. The reduction in E_{KE}, however, does not follow the same proportion, with the ratio of the first local maximum of E_{KE} for both cases ranging from 2.1 up to 2.6, depending on stringer geometry. This observation indicates the presence of nonlinearities in the simulations in virtue of the influence of damage on the constitutive equations that govern the response of the panels. Moreover, the influence of stringer geometry on the distribution of loads on the surface of the panels may affect the vibration modes of the panels.

The initial stiffness of the panels (prior to damage initiation) is the same, as every panel presents the same cross-sectional area. However, as damage initiates, the dynamic response of the panels depends on the extent and distribution of damage on the laminate. The reinforced panels shown a reduction of E_{DMD} from 27.7% (panel J) up to 50.9% (panel Ω), when compared to the maximum value of E_{DMD} of the panel without stringers at the instant of collapse. In general, for the panels in which the stringers withstand more damage, mainly associated with matrix crushing and cracking (T-, J- and Ω-shaped), less damage is found in the skin, with the exception of the J-shaped stringers, which show the highest values of damage on both skin and stringers (Figure 7).

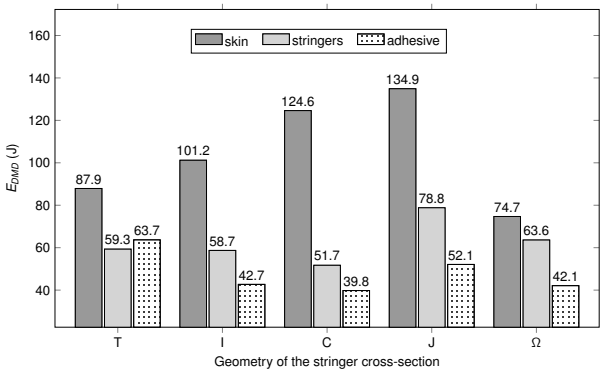

Figure 7: Energy dissipated by damage in the skin, stringers and adhesive interface for each configuration.

Additionally to the laminate damage model used, governed by Hashin's criteria, the damage on the adhesive interface in the form of debonding was modelled. Debonding started at sensibly the same time on the adhesive layer for every panel and was found to progress at different rates, depending on stringer configuration (which determines the surface contact areas and deformation modes). The values of E_{DMD} regarding the adhesive failure are proportional to the areas of contact of the stringer-skin interface (Figure 7). However, as the pressure loading from the shock wave exponentially decreases with time, the influence of full stringer-skin separation at latter stages of the blast event (Figure 8) becomes less important.

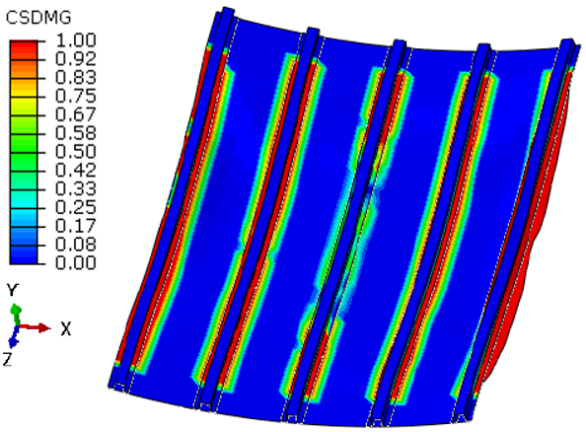

Figure 8: Failure on the adhesive interface (t = 2.0 ms).

Overall, it is shown that stringers present a viable solution to mitigate the effects of an explosive blast on curved CFRP panels. For the range of designs considered, the Ω-shaped stringers outperform the remaining configurations, showing the lowest global maximum out-of-plane displacement and least amount of structural damage.

5. Conclusions

A finite element model and analysis of carbon fibre-reinforced polymer (CFRP) laminate single-curved panels under blast loading was accomplished using the commercial software Abaqus/Explicit (version 6.14). The CONWEP model was used to simulate the shock wave loading from the explosive blast of a charge of TNT in free-air far-field conditions. The numerical model considered the in-plane mechanical properties of the composite laminate given by the matrix and fibres, which control the deformation and damage sustained by the panels. Damage in the laminate was modelled using the Hashin failure criteria, which assumes four different damage modes, comprising matrix and fibre failure with separate mechanisms for tension and compression. The modelling of the adhesive interface was accomplished through the implementation of a contact formulation based on the cohesive properties of the adhesive material and a maximum nominal stress criterion. An approach to qualitatively capture the strain-rate dependency in the composite material model allowed to assess the effects of blast-induced strain rates on the mechanical properties of the CFRP material.

The numerical study was able to capture the deformation history, failure modes and energy variation of the models. Additionally, the study of the influence of geometric parameters such as the curvature and stringers cross-section shape provided an insight on passive protective design alternatives capable of mitigating the effects of the dynamic loads during a bombing event. The proposed model can thus be used to design or evaluate the performance of blast resistant FRP composite structures under specific blast conditions.

References

[1] J. N. Reddy. *Mechanics of Laminated Composite Plates and Shells*, pages 81–83. CRC Press, 2^{nd} edition, 2004.

[2] C. Qi, S. Yang, L.-J. Yang, S.-H. Han, and Z.-H. Lu. Dynamic response and optimal design of curved metallic sandwich panels under blast loading. *The Scientific World Journal*, 07 2014.

[3] E. Wang, Q. Li, and G. Sun. Computational analysis and optimization of sandwich panels with homogeneous and graded foam cores for blast resistance. *Thin-Walled Structures*, 147, 02 2020.

[4] S. Li, X. Li, Z. Wang, G. Wu, G. Lu, and L. Zhao. Finite element analysis of sandwich panels with stepwise graded aluminum honeycomb cores under blast loading. *Composites Part A: Applied Science and Manufacturing*, 80:1 – 12, 2016.

[5] J. Shen, G. Lu, L. Zhao, and Z. Qu. Response of curved sandwich panels subjected to blast loading. *Journal of Performance of Constructed Facilities*, 25:382–393, 10 2011.

[6] A.P. Mouritz. Advances in understanding the response of fibre-based polymer composites to shock waves and explosive blasts. *Composites Part A: Applied Science and Manufacturing*, 125:105502, 2019.

[7] A. Gargano, K. Pingkarawat, M. Blacklock, V. Pickerd, and A.P. Mouritz. Comparative assessment of the explosive blast performance of carbon and glass fibre-polymer composites used in naval ship structures. *Composite Structures*, 171:306 – 316, 2017.

[8] A. Gargano, R. Das, and A.P. Mouritz. Finite element modelling of the explosive blast response of carbon fibre-polymer laminates. *Composites Part B: Engineering*, 177:107412, 2019.

[9] P. Kumar, D.S. Stargel, and A. Shukla. Effect of plate curvature on blast response of carbon composite panels. *Composite Structures*, 99:19 – 30, 2013.

[10] V. Karlos and G. Solomos. Calculation of blast loads for application to structural components. Technical report, Joint Research Center of the European Commission, 2013.

[11] S. Giversen. Blast testing and modelling of composite structures. Technical Report S167, DTU Mechanical Engineering, 2014.

[12] C. N. Kingery and G. Bulmash. Air blast parameters from tnt spherical air burst and hemispherical burst. Technical Report ARBRL-TR-02555, U.S. Army Ballistic Research Laboratory, 1984.

[13] Z. Hashin and A. Rotem. A fatigue failure criterion for fiber reinforced materials. *Journal of Composite Materials*, 7:448–464, 1973.

[14] Z. Hashin. Failure criteria for unidirectional fibre composites. *ASME Journal of Applied Mechanics*, 47(2):329 – 334, 1980.

[15] Dassault Systèmes. Abaqus/CAE User's Guide (6.14). Providence, RI, USA, 2014.

[16] R. Degenhardt, A. Kling, K. Rohwer, A.C. Orifici, and R.S. Thomson. Design and analysis of stiffened composite panels including post-buckling and collapse. *Computers Structures*, 86(9):919 – 929, 2008. Composites.

[17] G. Pereira. *Computational modelling of failure of stiffened composite panels*. MSc thesis in Aerospace Engineering, Instituto Superior Técnico, University of Lisbon, 2017.

[18] M. Silva. *Strength of aircraft composite panels under transverse impact loading*. MSc thesis in Aerospace Engineering, Instituto Superior Técnico, University of Lisbon, 2018.

[19] H. Martins. *Comportamento mecânico de painéis compósitos de fuselagem sujeitos a ações de impacto: Influência do projétil, carregamento e taxa de deformação*. MSc thesis in Aerospace Engineering, Instituto Superior Técnico, University of Lisbon, 2021.

[20] A. Winzen and R. Degenhardt. Simulation of stringer stiffened CFRP panels in consideration of skin-stringer separation. 04 2006.

[21] P.P. Camanho, P. Maimí, and C.G. Dávila. Prediction of size effects in notched laminates using continuum damage mechanics. *Composites Science and Technology*, 67(13):2715 – 2727, 2007.

[22] R. Krueger and P. Minguet. Analysis of composite panel-stiffener debonding using a shell/3D modeling technique. 01 2006.

[23] J.D. Schaefer, Brian Werner, and I.M. Daniel. Strain rate effects on failure of a toughened matrix composite. *Conference Proceedings of the Society for Experimental Mechanics Series*, 6:117–123, 07 2014.